Biomaterials 175 (2018) 72–81

Contents lists available at ScienceDirect

Biomaterials

journal homepage: www.elsevier.com/locate/biomaterials

Ingestible roasted barley for contrast-enhanced photoacoustic imaging in animal and human subjects

Depeng Wang [a], Dong Hyeun Lee [a], Haoyuan Huang [a], Tri Vu [a], Rachel Su Ann Lim [a], Nikhila Nyayapathi [b], Upendra Chitgupi [a], Maggie Liu [c], Jumin Geng [a], Jun Xia [a, *], Jonathan F. Lovell [a]

[a] Department of Biomedical Engineering, University at Buffalo, State University of New York, Buffalo, USA
[b] Department of Electrical Engineering, University at Buffalo, State University of New York, Buffalo, USA
[c] Department of Linguistics and Speech and Hearing Science, University at Buffalo, State University of New York, Buffalo, USA

ARTICLE INFO

Article history:
Received 26 February 2018
Received in revised form
10 May 2018
Accepted 11 May 2018
Available online 17 May 2018

Keywords:
Ingestible
Roasted barley
Photoacoustic tomography
Swallowing
Contrast agent

ABSTRACT

Photoacoustic computed tomography (PACT) is an emerging imaging modality. While many contrast agents have been developed for PACT, these typically cannot immediately be used in humans due to the lengthy regulatory process. We screened two hundred types of ingestible foodstuff samples for photoacoustic contrast with 1064 nm pulse laser excitation, and identified roasted barley as a promising candidate. Twenty brands of roasted barley were further screened to identify the one with the strongest contrast, presumably based on complex chemical modifications incurred during the roasting process. Individual roasted barley particles could be detected through 3.5 cm of chicken-breast tissue and through the whole hand of healthy human volunteers. With PACT, but not ultrasound imaging, a single grain of roasted barley was detected in a field of hundreds of non-roasted particles. Upon oral administration, roasted barley enabled imaging of the gut and peristalsis in mice. Prepared roasted barley tea could be detected through 2.5 cm chicken breast tissue. When barley tea was administered to humans, photoacoustic imaging visualized swallowing dynamics in healthy volunteers. Thus, roasted barley represents an edible foodstuff that should be considered for photoacoustic contrast imaging of swallowing and gut processes, with immediate potential for clinical translation.

1. Introduction

As a hybrid imaging modality that combines acoustic detection with optical excitation, photoacoustic computed tomograph (PACT) has proven capable of multiscale imaging with endogenous or exogenous contrasts, making it a valuable imaging tool in biomedical research [1,2]. The most commonly used endogenous contrast agent is hemoglobin, which provides anatomic [3,4], functional [5] and metabolic [6] information about blood vessels. Numerous exogenous agents for PACT have been demonstrated to enhance imaging contrast, including metallic nanoparticles [7–14], carbon nanotubes and graphene [15,16], organic semiconducting polymer nanoparticles [17–21], tetrapyrrole nanoparticles [22–24], dyes [25–29], proteins [30–32], and many others [33–36]. Compared to endogenous contrast agents, exogenous contrast agents can be designed to improve photoacoustic detection sensitivity or to reveal functional and molecular information such as intestine motility [37], glucose uptake [38], or calcium activity [39]. Unfortunately, with the exception of dyes such as indocyanine green, which are already approved for human use by health regulatory agencies, the majority of these novel contrast agents will not be tested in humans until passing through a lengthy and expensive regulatory process. A readily available and safe exogenous contrast agent that is already consumable would be attractive for improving immediate clinical applications of contrast-enhanced PACT. One imaging application for a consumable PACT contrast agent is swallowing imaging. Swallowing is a complex movement which is completed through coordination of nerves and muscles in the tongue, palate, pharynx, larynx, and esophagus. Swallowing disorders in humans can result in serious health issues. So far, swallowing testing in human has been performed through magnetic resonance imaging (MRI) [40], X ray [41], and ultrasound

* Corresponding author.
E-mail address: junxia@buffalo.edu (J. Xia).

https://doi.org/10.1016/j.biomaterials.2018.05.016
0142-9612/

imaging [42]. However, MRI is high in cost, X-ray is radiative and not suitable for long-term imaging, and ultrasound has difficulty in differentiating small amount of swallowed materials from tissues. PACT is low cost, non-radiative and sensitive to optical absorption contrast. With a consumable and absorptive contrast agent, PACT might be used as a new screening and/or diagnostic tool for swallowing disorders.

In this work, we examine foods as potential photoacoustic (PA) contrast agents. Roasted barley was identified through screening of already human-consumed, edible products and is demonstrated to be a viable contrast for PA imaging in animal and human subjects. This technique allowed swallowing processes to be characterized through PACT safely and non-invasively in humans for the first time. The wavelength we chose for imaging was 1064 nm, which is advantageous for deep tissue imaging for the following reasons: low optical scattering [43], homogeneous contrast from background tissue [44], high wall-plug laser output efficiency based on current laser technology, and high maximum permissible exposure value as defined by the American National Standards Institute (ANSI) [45].

2. Materials and methods

2.1. Photoacoustic computed tomography (PACT) system configuration

All experiments were performed with our customized PACT system that utilizes an Nd:YAG laser (Continuum) as an excitation source, whose output is 1064 nm light with 10 Hz pulse repletion rate and 10 ns pulse duration (Fig. 1a). As the imaged subjects varied in different experiments, selection of optical fiber bundles for light delivery and transducers for PA signal detection were carefully considered. Configurations of PACT system in all experiments are as follows: 1) PACT system equipped with L7-4 (ATL/Philips, linear transducer array with 128-element and 5 MHz center frequency) and bifurcated fiber bundle (one circular input and two linear outputs) was used in experiments of preliminary sample pool screening, agar phantom scan and mouse intestines mapping (Fig. 1, Fig. S1a); 2) PACT system equipped with L7-4 and circular fiber (both input and output were circular) was used in depth imaging through chicken breast tissue and human hand, and dynamics intestine imaging; 3) PACT system equipped with ring fiber and three-quarter-ring transducer array (custom-made, 128-element, 5 MHz center frequency) was used solely in final sample pool screening (Fig. S1b); 4) PACT system equipped with C5-2 (Philips C5-2, 128-element, center frequency 3 MHz) and bifurcated fiber was used only in human swallowing imaging (Fig. 1b). The coupling efficiency for all three aforementioned fibers is approximately 50%. The maximum light intensities at the object surface varied from 20 to 30 mJ/cm^2 in different experiments, but all are well below the ANSI safety limit (100 mJ/cm^2) at 1064 nm [45]. Signals detected by transducers were amplified and digitized by a 128-channel ultrasound data acquisition (DAQ) system (Vantage, Verasonics) with 20 MHz sampling rate and 54 dB gain (24 dB low noise amplifier + 30 dB programmable gain amplifier). After each laser pulse, the raw channel data was reconstructed using the universal back-projection algorithm [46] and was displayed in real-time during experiments.

2.2. Preliminary sample pool screening

In order to identify the potential candidates for PA imaging, 200 types of ingestible foodstuff samples were scanned with our PACT system (Fig. S1a). For scanning, we used a 96-well plate as a sample container. The plate is made of transparent plastic to ensure maximum light illumination to all samples. In each well, 50 mg of foodstuff was weighed and ~360 μL of water was added to achieve a concentration of 139 mg/mL. The plate was then sealed with a transparent plastic tape. To ensure illumination for the sample, neighboring wells were kept empty. The 1064 nm light of the laser was routed to the imaging region through a bifurcated optical fiber bundle. The light intensity at the surface of the plate surface was around 30 mJ/cm [2], which is below the ANSI safety limitation at 1064 nm. The plate was placed underneath a water tank with a bottom window, which was sealed with an optical and ultrasound transparent silicon film. Ultrasonic gel was applied as a coupling medium between plate surface and film. PA signal of the sample was acquired by a L7-4 transducer array, which was scanned with a 0.1 mm step size from the first to the final row of the plate. Because the width of the transducer array is 38 mm, only four columns of the well-plate can be imaged in one scan. Three scans were needed to image the whole plate.

2.3. Final sample pool screening

Final sample pool screening among 20 different roasted barleys was performed with our PACT system using a three-quarter ring transducer array (Fig. S1b). For each barley, 6 mL solution with

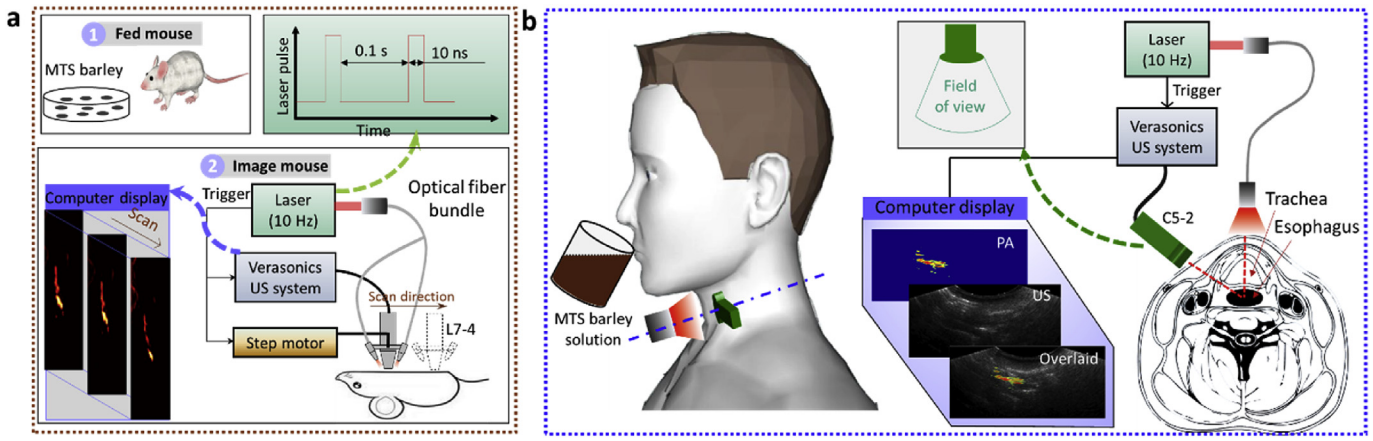

Fig. 1. PA imaging systems. (**a**). Schematic drawing of the setup used in mouse intestine imaging. The animal was fed with roasted barley before imaging. The transducer moved along the scan direction to acquire three-dimensional images. Trigger signals from the laser enabled synchronization among laser, DAQ and translation stage (driven by step motor). (**b**) Schematic drawing of the set up used for human swallowing imaging. Field of view of the C5-2 transducer is shown in the gray region.

50 mg/mL concentration was filled into a plastic bottle with a thin and transparent wall, permitting good light and ultrasound penetration. The sample was prepared with room temperature water and imaged immediately after preparation. Light delivery was provided by a 6-cm-diameter ring fiber illuminator (Light Source Flex Cable 12-Light Ring-Mount, Fiberoptic Specialties). Along the ring, twelve circular fiber outputs (0.3 cm in diameter) are evenly distributed and illuminated towards the center at a 60° angle (along the elevation direction). The light intensity at the bottle surface was around 30 mJ/cm [2], which is also below the ANSI safety limit at 1064 nm. Before the experiment, we adjusted the height of the ring fiber to ensure that the imaged cross-section receives maximum light energy. During the experiment, the bottle was scanned over 3 cm distance with a 0.1 mm step size at a speed of 1 mm/s. PA signals were detected by the three-quarter ring transducer array. The radius of the ring array was 40 mm and each element formed an elevation focus at 35 mm. Thus, elevation resolution and receiving sensitivity are relatively uniform at the central 10 mm radius region [47–49]. For each image, we ensured that the bottle is located within the field of view of the transducer. Signals from the transducer array were transmitted to the Vantage system through custom-made cables and connectors. With a matched number of DAQ channels and transducer elements, we can acquire a cross-sectional image of the bottle after each laser pulse. Muntons roasted black barley (MTS) was selected for further experiments.

2.4. Depth imaging though milk and chicken breast tissue

Two phantom experiments were performed with our linear transducer PACT system. For both experiments, the 1064 nm light was coupled to the circular fiber bundle (#39-371, Edmund Optics) and illuminate on the object surface. Light intensity over the 1.3-cm-diameter illuminated region was around 25 mJ/cm [2]. PA signals were detected by the L7-4 transducer.

First, roasted (MTS) barley was imaged through milk. The phantom is made of agar gel with hundreds of pearl and one roasted barley embedded. During the experiment, the phantom was immersed in a milk-filled tank and imaged in the same procedure as the preliminary sample pool screening experiment. The second phantom experiment is depth imaging through chicken breast tissue, whose optical properties are comparable to that of human breast [50]. The experimental procedure is similar to previous studies [49, 51]: A layer of roasted barley was placed on a piece of chicken tissue (5 cm in thickness), then we gradually stacked chicken breast tissues on top of barley until we could not detect any PA signals from barley. We also put a TYGON tube (4 mm inner diameter) filled with water and three roasted barley grains inside the chicken tissue, and then tracked the flow of barley granule.

2.5. Human thenar space imaging

Experiments were performed in compliance with the IRB protocol approved by the University at Buffalo. The transducer array used in the experiment was L7-4. One roasted (MTS) barley and one pearl barley grain were placed on top of a piece of intralipid and agar gel mixed phantom (3 cm in thickness), and the human thenar was put on top of two granules. Ultrasound gel was used in the experiment as a coupling medium. The gel was placed both under (coupling barley and hand) and on top of the hand (coupling hand and transducer). The 1064 nm laser output was routed to hand through the circular fiber bundle. The maximum light intensity at the skin surface was around 25 mJ/cm [2].

2.6. Mouse intestine imaging

All animal experiments were performed in compliance with the animal protocol approved by Institutional Animal Care and Use Committee at University at Buffalo. Before imaging, female ICR mice (18–22 g) were fasted overnight with water access, and then were provided with 5 g of roasted MTS barley or pearl barley for eating. Three hours later, we measured the remaining barleys to be 2.8–3.4 g, indicating that 1.6–2.2 g have been consumed by mice. After the hair of mice was shaved, their intestines were imaged photoacoustically using the L7-4 array (Fig. 1a). The light intensity at the skin surface of mice was controlled be to 20 mJ/cm^2. The scanning distance over the intestine region is 4 cm in the elevation direction. For dynamic intestine imaging, the transducer was parallel to the coronal plane of mice with their intestines in the imaging plane of the transducer. Light beam was delivered with the circular fiber bundle from top of intestines.

2.7. Human swallowing imaging

MTS barley (50 mg/mL) was boiled in water for 10 min, and the solution was put in room temperature (23 °C) to cool. We first imaged 50 μL of the liquid part of boiled barley tea (filled in a tube with 4 mm diameter) through 2.5 cm chicken breast tissue with the PACT configuration 2. The liquid part of the solution was separated from the solid part for experiment. Another tube filled with the same volume of PBS was also imaged for comparison. Then we performed human swallowing study. Human swallowing imaging was performed in compliance with the protocol approved by the University at Buffalo IRB committee. To achieve a large imaging field of view, we used a curved-transducer array (C5-2). A volume (10 mL) of the liquid part of barley tea was offered to subjects in a cup. After making sure that subject was comfortably arranged, he/she was instructed to hold the solution in the oral cavity for a few seconds and swallow after a command from the system operator. The transducer was positioned towards the pharynx/esophagus through the carotid vessel, which was a fluid-filled structure with minimal ultrasound attenuation. During the experiment, we slightly adjusted the transducer to obtain a longitudinal view of the pharynx/esophagus and to reveal the bolus of barley solution during swallowing. Light delivery was provided through the circular optical fiber bundle and the light intensity on the skin surface was approximately 30 mJ/cm [2], which takes only ~30% of the ANSI limit at 1064 nm (Fig. 1b).

3. Results and discussion

3.1. Screening foods for photoacoustic contrast

Because there are different types of food available, the major challenge for food contrast imaging is to identify candidates that produce strong PA signal at 1064 nm. For this task, we classified drinkable or edible foodstuffs into seven categories: tea, seed, coffee, chocolate, juice, vegetable and seasoning. With this classification as a guideline, 200 samples covering all those categories were purchased in their dry forms, such as garlic powder, roasted barley, and dry seed, and scanned with our linear-array-based PACT system (Fig. S1a).

Fig. 2 shows the images for preliminary sample pool scanning experiment. Fig. 2a is the photograph of one representative plate containing 42 food samples and a control sample. Food samples were placed in the first six rows, while a control sample [solution (2.8×10^{-4} mg/mL) of a near infrared (NIR) dye that is similar to a recently reported one [51]] with the absorbance of 0.5 (based on 1 cm path length) at 1064 nm was used for normalization. In total, five

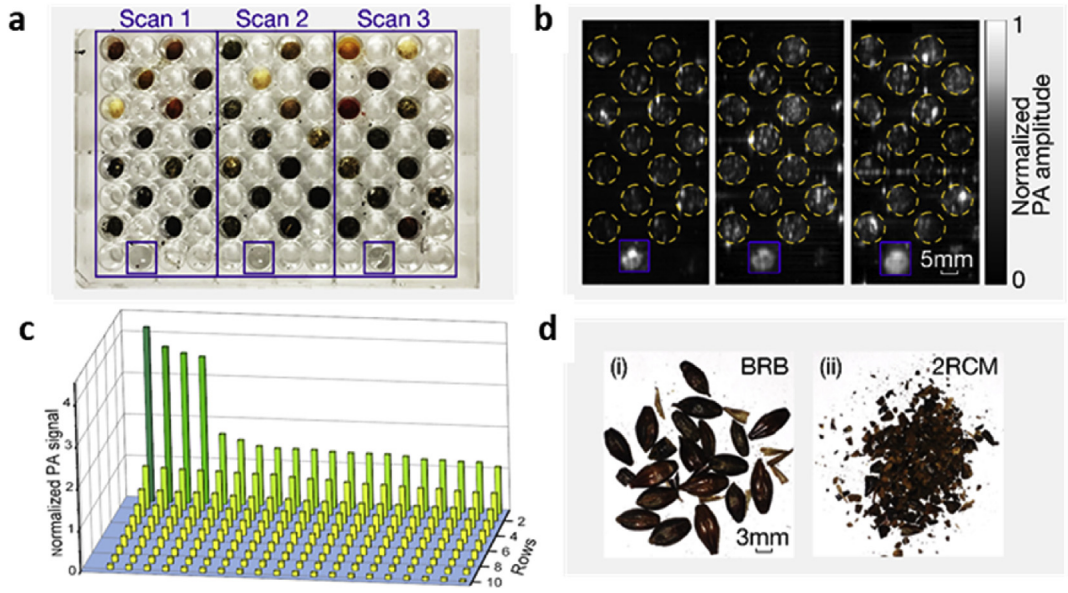

Fig. 2. Food screening identifies roasted barley as a potential candidate for photoacoustic contrast. (**a**) Photograph of a 96 well-plate filled with samples. Control samples are labeled with blue boxes. (**b**) PA image of well-plate filled with samples. Samples were normalized to a reference contrast agent shown in the blue box. (**c**) PA amplitude of 200 types of food samples and control in the preliminary scanning. (**d**) Photographs of top two samples (both roasted barley) identified in the preliminary screen. (For interpretation of the references to color in this figure legend, the reader is referred to the Web version of this article.)

plates were used to cover all samples (samples can be seen in Table S1). Representative maximum amplitude projections (MAP) image of one plate is shown in Fig. 2b. Wells containing samples with high absorbance at 1064 nm could be visualized with inhomogeneous areas of intense brightness, while wells filled with weak absorptive samples were only partially or barely observed. To quantify PA signals of all samples, we first averaged the signals within the well-plate area of each sample (both food samples and control). Then, we normalized the averaged signals of food with that of control in the same scan. The relative PA amplitudes of control and all samples are shown in Fig. 2c. Most samples produced lower PA amplitude than the NIR dye control sample, and only a small portion of samples exhibit higher signals. The top sample was BRB (Briess roasted barley), whose signal was 4.2 times compared to that of the 1064 nm reference dye and 13% higher than that of the second sample (2RCM: 2-row malt roasted barley). Both these "hits" were types of roasted barley. This experiment indicates that roasted barley could be a promising photoacoustic contrast agent. Photographs of the top two samples are shown in Fig. 2d, all of which appear dark, from their roasting process.

3.2. Roasted barley screening

In preliminary sample pool screening, roasted barley showed the strongest PA signal at 1064 nm. Then, we refined our study to only roasted barley, and imaged 20 different types of commercial roasted barley granules or powder solutions with our three-quarter ring transducer based PACT system (Fig. S1b) [48,49]. As the coverage angle of three-quarter ring transducer is 270°, this system could reveal barley grains distributed in any directions. The control sample used was the same as the preliminary sample screening. Each barley or control solution was filled in a soft and transparent plastic bottle with a thin (0.15 mm) wall, which allows good light illumination and ultrasound signal transmission. Fig. 3a shows two bottles filled with MTS (Muntons roasted black barley, unmalted) barley with or without grains. Different cross-sections of the bottle were imaged by scanning it horizontally. The MAP of all cross-sections reveals granules located at different depths (Fig. 3b). In contrast, minimal signals were observed in MAP image of the bottle without any grains. This demonstrates that barley granule is the main contributor to PA signals. Because of light attenuation, granules located close to the bottle surface exhibit stronger PA signals than those in the center region. For a fair comparison, we quantified the average PA amplitude within a 3-mm donut-shaped region (green circles in Fig. 3b) and normalized that with the control sample. The PA amplitude rankings for all samples are shown in Fig. 3c. For simplicity, we list the abbreviated name for each sample. Full names of samples can be found in Table S2. It can be seen in Fig. 3c that only the MTS solution with grains gives the highest normalized PA amplitude (5.3), which is more than 5 times to that of control and 29% higher than that of the top one sample in Fig. 2c. Thus, MTS barley exhibits the highest PA signal among all the food samples. Therefore, we used MTS barley for all subsequent experiments. Photographs of the top three samples in this experiment can be found in Fig. 3c inset (i-iii). As can be seen in the photographs, different roasted barley brands have different physical parameters including the average grain size. Roasting time and processing steps such as grinding could likely induce changes in how the roasted barley tea behaves in tea formation and PACT imaging. In this study, we simply used the roasted barley as is without any modification, although exploration of barley size warrants investigation. Additionally, it may be of interest to also consider the development of nanoscale formulations of roasted barley. A recent report showed that nanoparticles can be formed from roasted bamboo, following a grinding and sonication process for drug loading and photothermal therapy [52].

Fig. 3c(iv) shows the absorbance of the liquid phase of prepared MTS in the NIR region (700–1100 nm). Within this wavelength range, the ANSI limit increases from 700 nm to 1050 nm and then stays constant until 1100 nm. Because PA amplitude is proportional to the product of absorbance and light intensity, the green curve in Fig. 3c(iv) represents the expected PA amplitude acquired under maximum permissible illumination. It can be seen that 1064 nm is close to the peak wavelength in the curve.

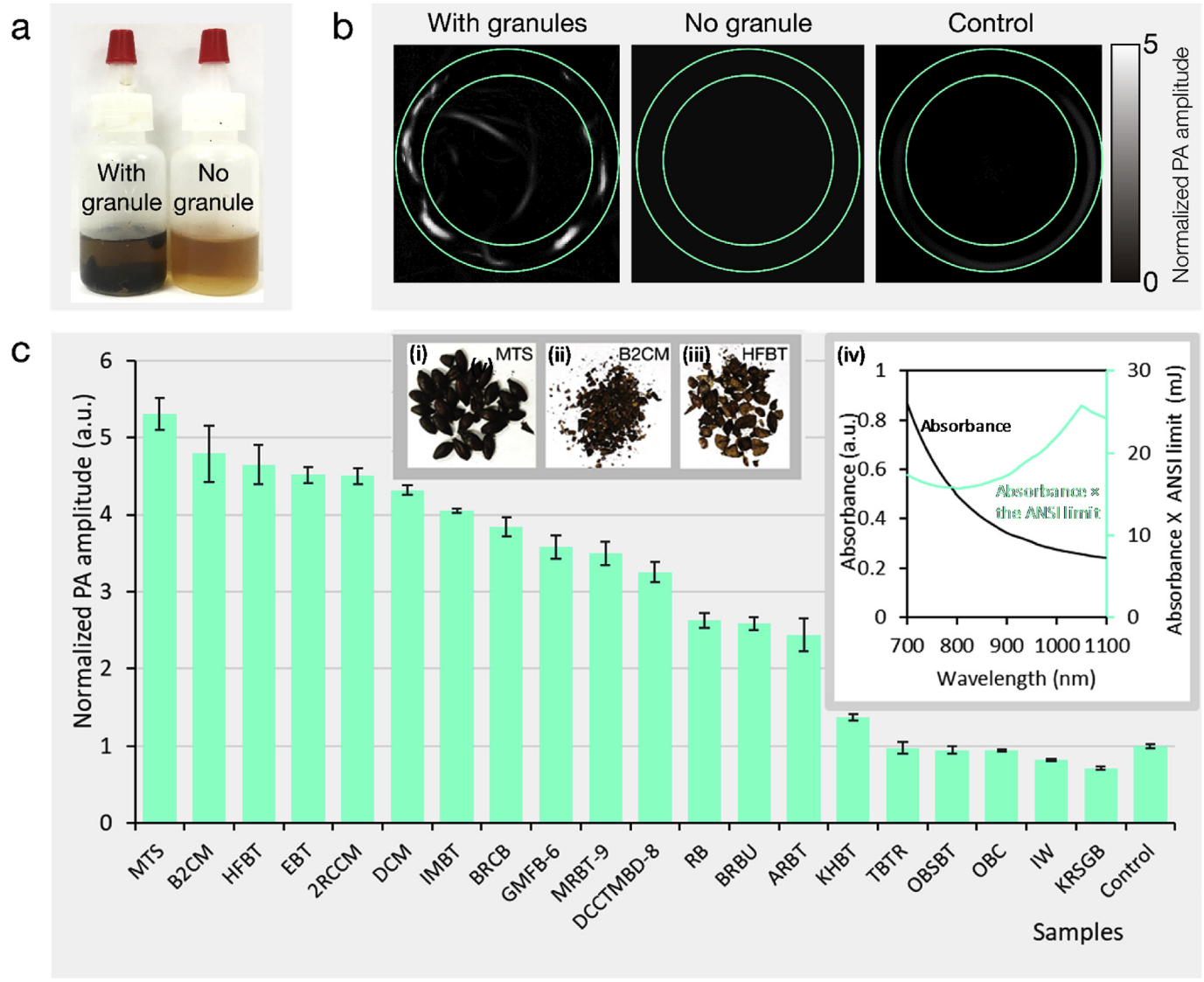

Fig. 3. Photoacoustic screening of commercial roasted barley. (**c**) Photograph of bottles filled with MTS barley solutions with and without granules. (**b**) MAP of PA images for MTS barley (with and without barley grains) and control sample. (**c**) PA amplitudes of roasted barleys and control sample. **Inset (i-iii)** Photographs of the top three barleys: MTS, B2CM (Briess 2 row chocolate malt), and HFBT (House food barley tea DC), respectively. **Inset (iv)** Absorbance of the liquid portion of MTS in the NIR region (black curve) and the product of MTS's absorbance and ANSI limit (green curve). Mean ± s.d. for n = 3 bottles. (For interpretation of the references to color in this figure legend, the reader is referred to the Web version of this article.)

3.3. Depth imaging in phantom

To assess the detection depth of using roasted (MTS) barley and PACT, we performed two phantom experiments: imaging of roasted barley through milk and chicken breast tissue. For the first experiment, milk was utilized as an imaging/coupling medium because it mimics scattering of biological tissue [53] and 3D scanning can be easily performed in milk. For the second experiment, we only performed 2D imaging and used chicken breast tissue to mimic both scattering and absorption of human tissue. Fig. 4a shows the phantom used in depth imaging through milk. Barley grains were clearly shown before the phantom was immersed in milk, whereas they cannot be seen after that. The distance from the transducer and optical fiber bundle to the phantom is around 3 cm. With linear scanning of the L7-4 transducer array, we acquired both ultrasound (US) and PA images of the phantom. The MAP of US image shows all the barley granules because they all reflect US signals. However, in the MAP of PA image, only the roasted barley granule stands out among all the barleys (Fig. 4b). This experiment proved that roasted barley can be easily recognized in PA, but not in US imaging among a group of granules. This underscores the capacity of roasted barley and photoacoustic imaging to be used to specifically detect the contrast in a biological environment. This data also shows that the roasting process specifically confers photoacoustic contrast to barley grains.

Roast (MTS) barley was compared to pearl barley in Fourier-transform infrared spectroscopy (FTIR) analysis (Fig. 4c). The roasted barley had distinct absorption around 2100 cm^{-1}, which represents an alkenyl C=C stretch. The more intense absorption around 1000-1500 cm^{-1} demonstrates chemical changes occur during the roasting process, and could correspond to modified or polymerized and aromatic groups. Further insight into the chemical nature of roasted barley was not elucidated in this study. Graphene oxide, which has photoacoustic properties was recently identified as a component in roast chicken [54]. Photoacoustic spectroscopy has been used for characterization of roasted coffee beans [55,56]. It

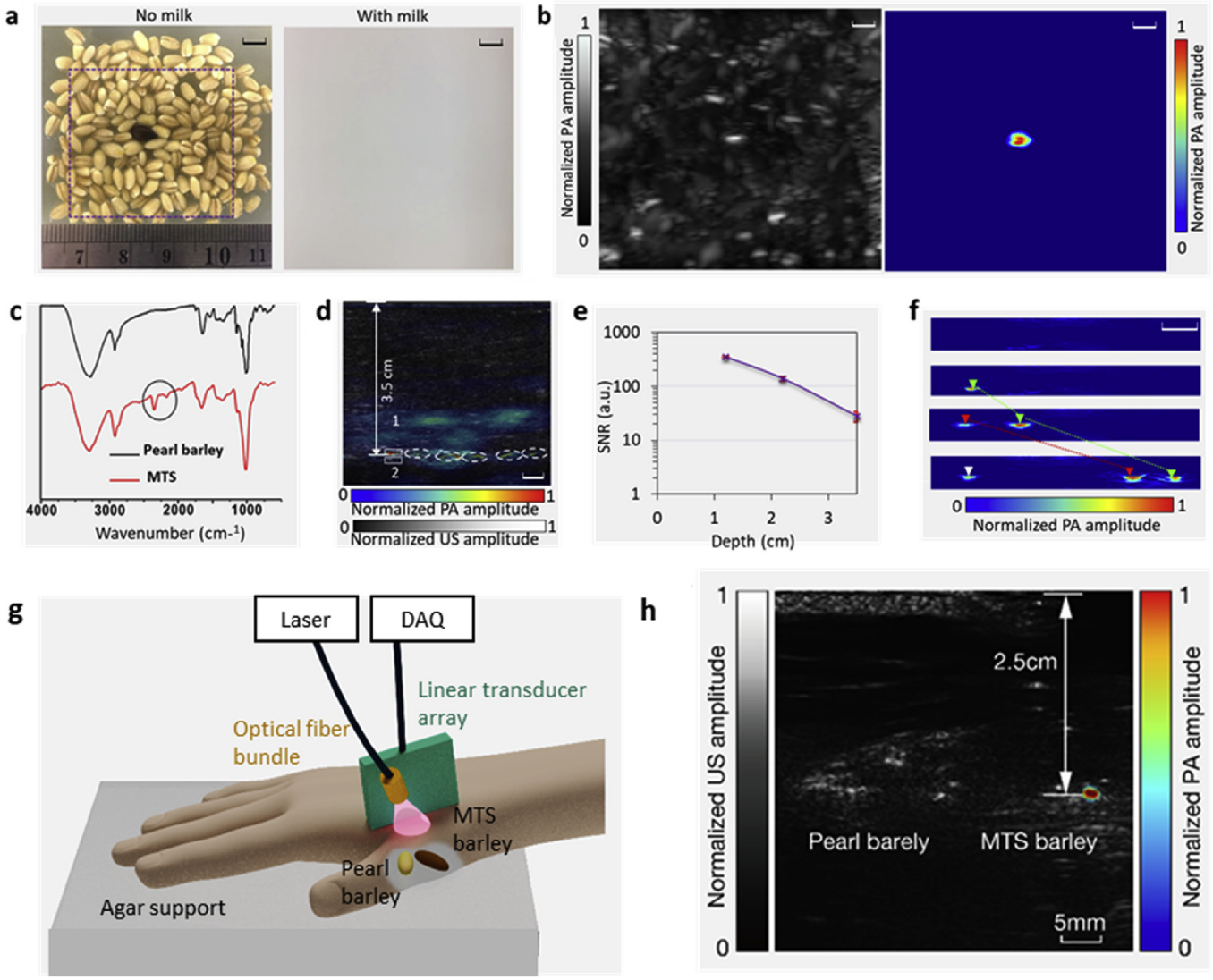

Fig. 4. Photoacoustic imaging of roasted barley (MTS). (**a**) Photograph of agar phantoms before (left) and after (right) being immersed in milk. The red dashed box shows the imaging region. (**b**) Left: US image of the agar phantom. Right: PA image of the agar phantom. (**c**) FTIR spectra of roasted barley (MTS) and unroasted pearl barley. The circle's absorption represents alkynyl stretches (C═C). (**d**) PA (color scale) overlaid US (gray scale) image for MTS barley imaging through chicken tissue. Barleys are marked with circles. (**e**) SNR of roasted barley PA signals at different depths. Error bars indicate standard deviations of 3 different quantifications. (**f**) PA images showing the movement of roasted barley granules. Scale bar is 5 mm. (**g**) Schematic drawing of the setup for thenar space imaging. (**h**) Representative result of one adult volunteer. The ultrasound image is plotted in gray while the thresholded PA image is plotted in color. The signal of roasted (MTS) barley was clearly visible under the thenar space. The distance between barleys and skin surface was 2.5 cm, which is the transmitting distance for PA signals. (For interpretation of the references to color in this figure legend, the reader is referred to the Web version of this article.)

is likely that numerous roasted foods could be potential candidates for photoacoustic contrast imaging. An advantage of roasted barley is that it is an inexpensive and commonly available roast foodstuff that is free of nervous system stimulant activity (i.e. like coffee or tea).

Then, we imaged roasted (MTS) barley through chicken breast tissue. To quantify the imaging depth, we gradually stacked chicken breast tissues on top of roasted barley and monitored the PA signal in real time. As the tissue thickness increased, roasted barley's PA signal decreased gradually and was eventually buried in background noise (without averaging) when the depth reached approximately 3.5 cm (measured with a ruler). We then stopped stacking chicken breast tissue, and considered this distance as the deepest detection depth. One hundred frames were acquired at this depth, and all the data were averaged to improve the signal to noise ratio (SNR). The PA overlaid US image is shown in Fig. 4d, in which the several roasted barley granules are visible. Distance from the tube to transducer surface was calculated to be 3.5 cm. Considering 50% energy loss through fiber coupling, the imaging depth could be even higher if we use fused silica optical fiber bundles [up to 80% coupling efficiency and the light intensity on the chicken surface would be 40 mJ/cm^2] or free-space light illumination (50 mJ/cm^2). After one hundred times averaging, the SNR at different imaging depths was quantified using the following formula: SNR $= \frac{\mu}{\sigma}$, where μ represents the mean values of signals within box 1 and σ is the standard deviation of signals within box 2 (a region contains mainly the background signal). The calculated SNR is shown in Fig. 4e. As expected, the value decreases as the depth increases. When a tube with three barley granules was placed 2.5 cm beneath the chicken tissue, we used a syringe to push the barley granule to move at a

speed of 5 mm/s. Interestingly, we were able to track the movement of the three roasted barley granules (Fig. 4f). Those results reveal the feasibility of roasted barley for dynamic imaging in deep tissue.

3.4. Human thenar space imaging

To demonstrate the translational potential of PACT using roasted barley as a contrast agent for deep tissue imaging, we tried to image roasted (MTS) barley through a human hand. To avoid acoustic distortion from hand bones, we imaged through the thenar region. One pearl barley (low absorbance) and one roasted barley were placed beneath the thenar of a healthy adult human (Fig. 4g). With our Verasonics system, we collected both US and PA data. When the thenar was first imaged without any barley underneath, no clear PA signal was observed even after 100 times averaging. When pearl and roasted barley were placed under the thenar portion of the hand, roasted barley could be clearly seen with PACT through 2.5 cm of thenar (Fig. 4h). However, pearl barley was not seen. In this experiment, the energy applied to the skin surface is only 30 mJ/cm [2], a fraction of the ANSI safety limit.

3.5. Dynamic imaging of animal intestine

Roasted barley was then assessed as an intestinal imaging contrast agent for PACT *in vivo* in mice. Before imaging, three mice were fed with pearl barley while another three were fed with roasted (MTS) barley. Using our linear array based PACT system, we mapped the intestines of all mice. The laser intensity was controlled to be 30 mJ/cm^2 on the skin surface of mice (a fraction of ANSI limit). Minimal PA signals were observed in the mice fed with pearl barley. In contrast, intestines of the mice fed with roasted barley are clearly seen (Fig. 5a). Depth encoded PA image reveals intestine depth of up to 5 mm. Then, we tracked the intestinal dynamic motion of these mice, at a rate of 10 frames per second, which is much faster than the 0.5 Hz intestine peristalsis rate. To mitigate motion artifacts caused by respiration, we computed the covariance matrix of all image frames, identified ones with the largest body displacement (based on amplitudes of the eigenvector [57]), and replaced those frames with neighboring averages. Representative frames are shown in Fig. 5b (Movie S1), in which the transition of roasted barley within the white box can be clearly identified. The peristaltic rate was calculated based on the average signal amplitude within the white box (Fig. 5c). Fifteen peaks could be identified within 30 s, indicating a peristaltic rate of 30 per minute, which is the expected rate in mice under anesthesia. For better illustration, the peristaltic rate was calculated over time (Fig. 5d) and the result agrees with Fig. 5c. We also imaged feces of the mice fed with roasted and pearl barleys. The PA amplitude for feces of mice fed with roasted barley was up to 6 times stronger compared to that of the mice fed with pearl barley (Fig. 5e). All these results demonstrate that roasted barley is an effective contrast agent for imaging of intestine motility.

Supplementary video related to this article can be found at https://doi.org/10.1016/j.biomaterials.2018.05.016.

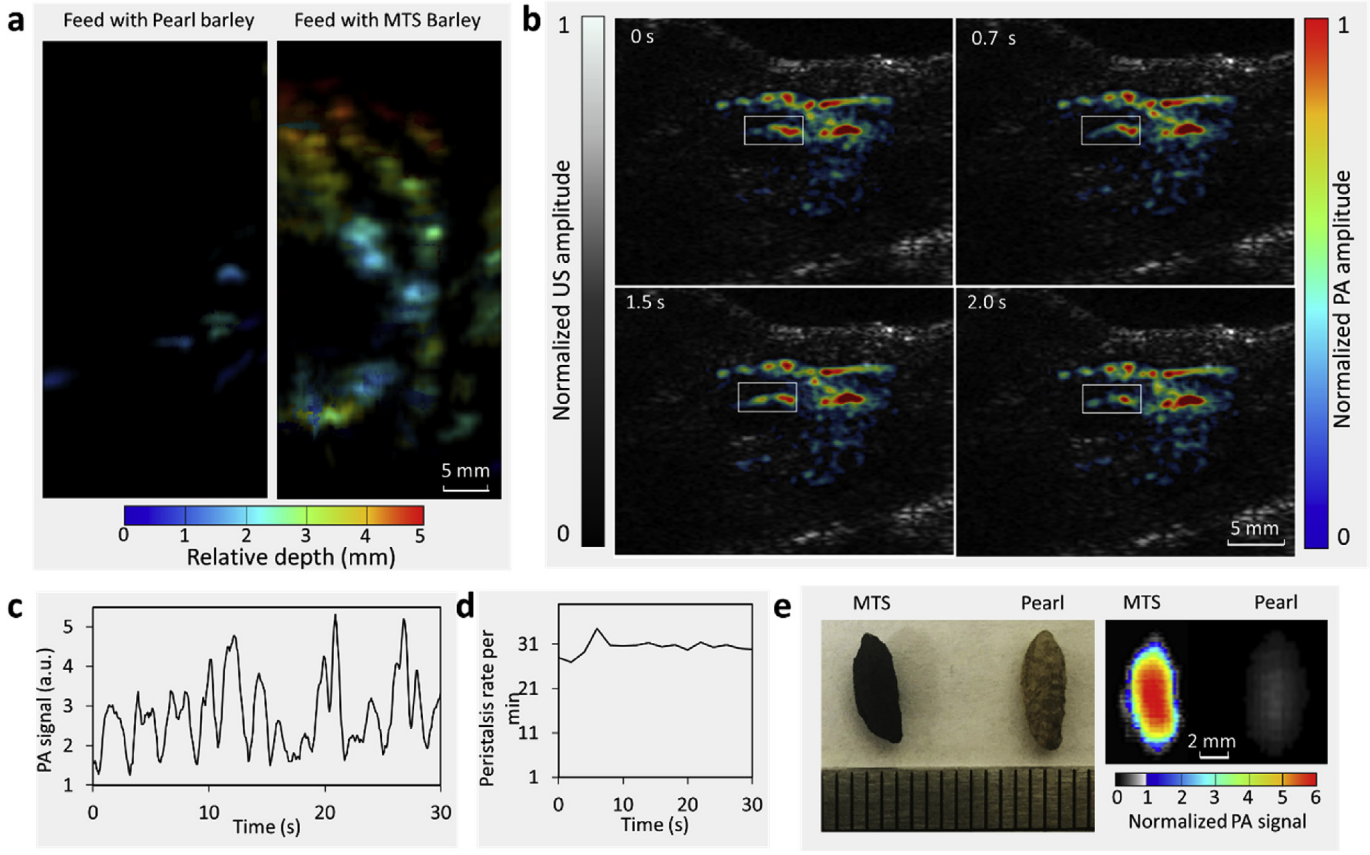

Fig. 5. Dynamic imaging of intestine. (**a**) PA intestine image for mice fed with pearl (left) or roasted (MTS) barley (right). (**b**) Representative PA (color scale) and US (gray scale) images show mouse intestine peristalsis. (**c**) Averaged PA signals within white boxes in (b) over 30 s. (**d**) Quantification of peristaltic rate over 30 s. (**e**) Photograph (left) and PA image (right) for feces of mice fed with roasted (MTS) or pearl barley. (For interpretation of the references to color in this figure legend, the reader is referred to the Web version of this article.)

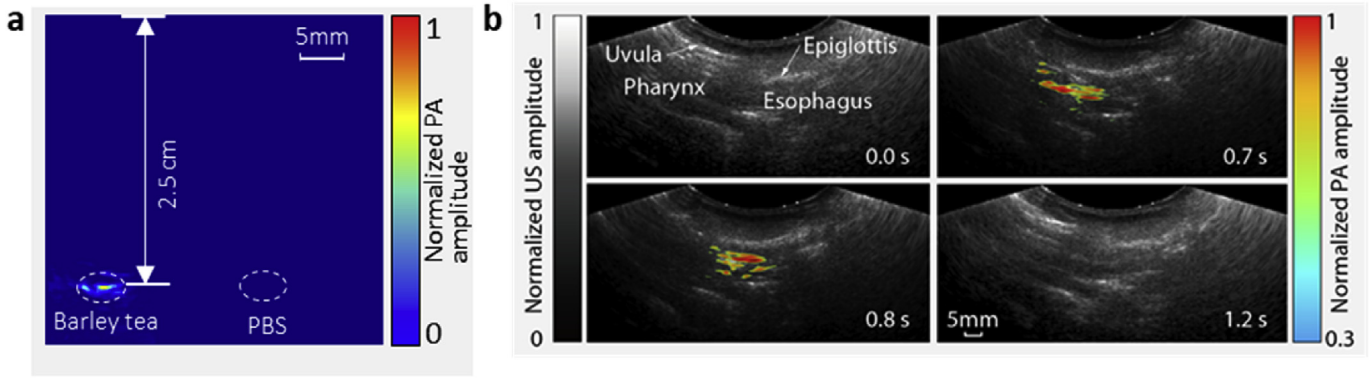

Fig. 6. Imaging of boiled barley tea in phantoms and in healthy human volunteers. (**a**) Imaging of 50 μL barley tea through 2.5 cm chicken breast tissue. (**b**) Overlaid PA (color) and US (gray) images for human swallowing in healthy volunteers. A threshold was applied to (b): values below that threshold (0.3) were not shown (Movie S2). (For interpretation of the references to color in this figure legend, the reader is referred to the Web version of this article.)

3.6. Swallowing imaging

Next, we used the liquid part of boiled barley tea as a contrast agent for real-time PA swallowing imaging. Swallowing is a complex sensorimotor process involving a coordinated neural interplay at cortical level [58]. Damage to this system can lead to swallowing problems (dysphagia). It is usually observed through techniques such as Video Fluoroscopic Swallowing Exam (VFSE) [59] and ultrasound [42,60,61]. However, those methods either contain ionization radiation (VFSE) or have low contrast in differentiating food residues from tissue (ultrasound). In this study, we report the first PACT evaluation of the swallowing process, using liquid part of boiled barley tea. Before the human study, we successfully detected 50 μL of the liquid part of boiled barley tea through 2.5 cm chicken breast tissue (Fig. 6a). This result demonstrated that boiled barley tea has potential for PACT of dysphagia which is related to liquid spill in trachea during swallowing. As a proof of concept, we imaged a healthy subject, using a C5-2 curved transducer array, which has a larger field of view than that of the linear array (L7-4). For better visualization, we also acquired US data to show the anatomical structure. Before swallowing, the participant held roasted barley solution in the oral cavity (oral preparatory stage) [62]. After receiving a command from the operator, the participant started swallowing. Sequentially, the second stage (oral propulsive stage) of swallowing happens. At this stage, the bolus was in oral cavity while transducer was detecting pharynx and esophagus regions, thus, no PA signal was shown in Fig. 6b (0.0 s). In the third (pharynx) and fourth (esophagus) stages of swallowing, the bolus passed through the pharynx and upper esophagus sequentially, and was clearly shown in Fig. 6b (0.7s, 0.8s), respectively. Thus, our method of using foodstuffs as a contrast agent enabled the first real-time PA swallowing imaging, indicating its potential for clinical applications.

Supplementary video related to this article can be found at https://doi.org/10.1016/j.biomaterials.2018.05.016.

4. Conclusions

We report the use of roasted barley as a safe and comestible PA contrast agent. Roasted (MTS) barley enables up to 3.5 cm imaging depth through chicken breast tissue and human thenar. It provides high recognizable PA signals among hundreds of non-roasted barley grains through a scattering medium. Roasted barley also showed promising PA results in animal and human studies. After feeding roasted barley to mice, we could noninvasively map intestines, and track the peristaltic rate. While tracking dynamic changes of mice intestines through PACT has been demonstrated several times in other studies [37,51], they utilized synthesized contrast agents whose availability is still limited and the timeline for clinical translation is unclear. In contrast, roasted barley is widely available in the market and could achieve the same tracking effect as synthetic contrast agents. Roasted barley also enabled the first PA imaging of the human swallowing process by showing the bolus with limited background noise. This spares the subject from ionizing radiation associated with swallowing imaging modality (VFSE). Due to the low pulse repetition rate of our laser, our frame rate for swallowing imaging is only 10 Hz, which is lower than the typical imaging frame rate (25 Hz) of VFSE. This issue can be addressed by using higher repetition rate lasers (50 Hz high-power pulsed lasers are commercially available). Currently, because we utilized only one transducer array, only the vertical section of the neck can be imaged during swallowing. To extend the field of view, we can employ multiple transducer arrays or design a cylindrical transducer array for swallowing assessment. Besides human swallowing imaging, roasted barley may potentially be used for clinical imaging to diagnose GI motility disorders such as esophageal achalasia, esophageal spasm, and esophageal reflux, as well as gastric motility disorders. Taken together, research of using roasted barley or other foods as contrast agents should open new avenues for PACT biomedical applications.

Data availability

All data is available upon request.

Acknowledgements

This work was supported in part by the National Institutes of Health grant DP5OD017898, Clinical and Translational Science Institute (CTSI) Pilot Studies Award, and University at Buffalo IMPACT award. All authors declare no competing financial interests.

Appendix A. Supplementary data

Supplementary data related to this article can be found at https://doi.org/10.1016/j.biomaterials.2018.05.016.

References

[1] D. Wang, Y. Wu, J. Xia, Review on photoacoustic imaging of the brain using nanoprobes, Neurophotonics 3 (1) (2016), 010901.
[2] L.V. Wang, J. Yao, A practical guide to photoacoustic tomography in the life sciences, Nat. Methods 13 (8) (2016) 627–638.

[3] D. Wang, Y. Wang, Y. Zhou, J.F. Lovell, J. Xia, Coherent-weighted three-dimensional image reconstruction in linear-array-based photoacoustic tomography, Biomed. Optic Express 7 (5) (2016) 1957–1965.
[4] J. Xia, M.R. Chatni, K.I. Maslov, Z. Guo, K. Wang, M.A. Anastasio, L.V. Wang, Whole-body ring-shaped confocal photoacoustic computed tomography of small animals in vivo, J. Biomed. Optic. 17 (5) (2012), 050506.
[5] J. Yao, L. Wang, J.-M. Yang, K.I. Maslov, T.T. Wong, L. Li, C.-H. Huang, J. Zou, L.V. Wang, High-speed label-free functional photoacoustic microscopy of mouse brain in action, Nat. Methods 12 (5) (2015) 407–410.
[6] R. Cao, J. Li, B. Ning, N. Sun, T. Wang, Z. Zuo, S. Hu, Functional and oxygen-metabolic photoacoustic microscopy of the awake mouse brain, Neuroimage 150 (2017) 77–87.
[7] W. Li, X. Chen, Gold nanoparticles for photoacoustic imaging, Nanomedicine 10 (2) (2015) 299–320.
[8] Y. Liu, J. He, K. Yang, C. Yi, Y. Liu, L. Nie, M. Khashab Niveen, X. Chen, Z. Nie, Folding up of gold nanoparticle strings into plasmonic vesicles for enhanced photoacoustic imaging, Angew. Chem. 127 (52) (2015) 16035–16038.
[9] X. Cheng, R. Sun, L. Yin, Z. Chai, H. Shi, M. Gao, Light-triggered assembly of gold nanoparticles for photothermal therapy and photoacoustic imaging of tumors in Vivo, Adv Mater. 29 (6) (2017), 1604894.
[10] S. Liang, C. Li, C. Zhang, Y. Chen, L. Xu, C. Bao, C. Wang, G. liu, F. zhang, D. Cui, CD44v6 monoclonal antibody-conjugated gold nanostars for targeted photoacoustic imaging and plasmonic photothermal therapy of gastric cancer stem-like cells, Theranostics 5 (9) (2015) 970–984.
[11] R. Cheheltani, R.M. Ezzibdeh, P. Chhour, K. Pulaparthi, J. Kim, M. Jurcova, J.C. Hsu, C. Blundell, H.I. Litt, V.A. Ferrari, H.R. Allcock, C.M. Sehgal, D.P. Cormode, Tunable, biodegradable gold nanoparticles as contrast agents for computed tomography and photoacoustic imaging, Biomaterials 102 (2016) 87–97.
[12] D. Dumani, I.-C. Sun, S. Emelianov, Detection of lymph node metastasis using photoacoustic imaging and glycol-chitosan-coated gold nanoparticles, J. Acoust. Soc. Am. 143 (3) (2018), 1930-.
[13] T. Repenko, A. Rix, A. Nedilko, J. Rose, A. Hermann, R. Vinokur, et al., Strong photoacoustic signal enhancement by coating gold nanoparticles with melanin for biomedical imaging, Adv. Funct. Mater. 28 (7) (2017), 1705607.
[14] G. Ku, M. Zhou, S. Song, Q. Huang, J. Hazle, C. Li, Copper sulfide nanoparticles as a new class of photoacoustic contrast agent for deep tissue imaging at 1064 nm, ACS Nano 6 (8) (2012) 7489–7496.
[15] A. De La Zerda, C. Zavaleta, S. Keren, S. Vaithilingam, S. Bodapati, Z. Liu, et al., Carbon nanotubes as photoacoustic molecular imaging agents in living mice, Nat. Nanotechnol. 3 (2008) 557.
[16] Z. Sheng, L. Song, J. Zheng, D. Hu, M. He, M. Zheng, G. Gao, P. Gong, P. Zhang, Y. Ma, L. Cai, Protein-assisted fabrication of nano-reduced graphene oxide for combined in vivo photoacoustic imaging and photothermal therapy, Biomaterials 34 (21) (2013) 5236–5243.
[17] Y. Lyu, J. Zeng, Y. Jiang, X. Zhen, T. Wang, S. Qiu, X. Lou, M. Gao, K. Pu, Enhancing both biodegradability and efficacy of semiconducting polymer nanoparticles for photoacoustic imaging and photothermal therapy, ACS Nano 12 (2) (2018) 1801–1810.
[18] Y. Jiang, P.K. Upputuri, C. Xie, Y. Lyu, L. Zhang, Q. Xiong, M. Pramanik, K. Pu, Broadband absorbing semiconducting polymer nanoparticles for photoacoustic imaging in second near-infrared window, Nano Lett. 17 (8) (2017) 4964–4969.
[19] C. Xie, P.K. Upputuri, X. Zhen, M. Pramanik, K. Pu, Self-quenched semiconducting polymer nanoparticles for amplified in vivo photoacoustic imaging, Biomaterials 119 (2017) 1–8.
[20] J. Li, J. Rao, K. Pu, Recent progress on semiconducting polymer nanoparticles for molecular imaging and cancer phototherapy, Biomaterials 155 (2018) 217–235.
[21] Y. Jiang, K. Pu, Advanced photoacoustic imaging applications of near-infrared absorbing organic nanoparticles, Small 13 (2017), 1700710 (1–19).
[22] Y. Zhang, D. Wang, S. Goel, B. Sun, U. Chitgupi, J. Geng, H. Sun, E. Barnhart Todd, W. Cai, J. Xia, J.F. Lovell, Surfactant-Stripped frozen pheophytin micelles for multimodal gut imaging, Adv. Mater. 28 (38) (2016) 8524–8530.
[23] Y. Zhang, H. Hong, B. Sun, K. Carter, Y. Qin, W. Wei, et al., Surfactant-stripped naphthalocyanines for multimodal tumor theranostics with upconversion guidance cream, Nanoscale 9 (10) (2017) 3391–3398.
[24] J.F. Lovell, C.S. Jin, E. Huynh, H. Jin, C. Kim, J.L. Rubinstein, W.C.W. Chan, W. Cao, L.V. Wang, G. Zheng, Porphysome nanovesicles generated by porphyrin bilayers for use as multimodal biophotonic contrast agents, Nat. Mater. 10 (2011) 324.
[25] D. Wang, Y. Wang, Y. Zhou, J.F. Lovell, J. Xia, Coherent-weighted three-dimensional image reconstruction in linear-array-based photoacoustic tomography, Biomed. Optic Express 7 (5) (2016) 1957–1965.
[26] H. Huang, D. Wang, Y. Zhang, Y. Zhou, J. Geng, U. Chitgupi, T.R. Cook, J. Xia, J.F. Lovell, Axial PEGylation of tin octabutoxy naphthalocyanine extends blood circulation for photoacoustic vascular imaging, Bioconjugate Chem. 27 (7) (2016) 1574–1578.
[27] X. Wang, G. Ku, M.A. Wegiel, D.J. Bornhop, G. Stoica, L.V. Wang, Noninvasive photoacoustic angiography of animal brains in vivo with near-infrared light and an optical contrast agent, Opt. Lett. 29 (7) (2004) 730–732.
[28] K. Jasung, J. Mansik, O. Yunok, K. Hyun Wook, K. Jeehyun, K. Chulhong, O. Junghwan, In vivo non-ionizing photoacoustic mapping of sentinel lymph nodes and bladders with ICG-enhanced carbon nanotubes, Phys. Med. Biol. 57 (23) (2012) 7853.
[29] Q. Chen, X. Liu, J. Zeng, Z. Cheng, Z. Liu, Albumin-NIR dye self-assembled nanoparticles for photoacoustic pH imaging and pH-responsive photothermal therapy effective for large tumors, Biomaterials 98 (2016) 23–30.
[30] J. Yao, A.A. Kaberniuk, L. Li, D.M. Shcherbakova, R. Zhang, L. Wang, G. Li, V.V. Verkhusha, L.V. Wang, Multi-scale photoacoustic tomography using reversibly switchable bacterial phytochrome as a near-infrared photochromic probe, Nat. Methods 13 (1) (2016) 67.
[31] S. Filonov Grigory, A. Krumholz, J. Xia, J. Yao, V. Wang Lihong, V. Verkhusha Vladislav, Deep-tissue photoacoustic tomography of a genetically encoded near-infrared fluorescent probe, Angew. Chem. Int. Ed. 51 (6) (2011) 1448–1451.
[32] A.P. Jathoul, J. Laufer, O. Ogunlade, B. Treeby, B. Cox, E. Zhang, P. Johnson, A.R. Pizzey, B. Philip, T. Marafioti, M.F. Lythgoe, R.B. Pedley, M.A. Pule, P. Beard, Deep in vivo photoacoustic imaging of mammalian tissues using a tyrosinase-based genetic reporter, Nat. Photon. 9 (2015) 239.
[33] G.P. Luke, D. Yeager, S.Y. Emelianov, Biomedical applications of photoacoustic imaging with exogenous contrast agents, Ann. Biomed. Eng. 40 (2) (2012) 422–437.
[34] J.E. Lemaster, J.V. Jokerst, What is new in nanoparticle-based photoacoustic imaging? Wiley Interdiscip. Rev. Nanomed. Nanobiotechnol. 9 (1) (2017).
[35] C. Kim, C. Favazza, L.V. Wang, Vivo photoacoustic tomography of chemicals: high-resolution functional and molecular optical imaging at new depths, Chem. Rev. 110 (5) (2010) 2756–2782.
[36] J. Weber, P.C. Beard, S.E. Bohndiek, Contrast agents for molecular photoacoustic imaging, Br. J. Pharmacol. 13 (2016) 639.
[37] Y. Zhang, M. Jeon, L.J. Rich, H. Hong, J. Geng, Y. Zhang, S. Shi, T.E. Barnhart, P. Alexandridis, J.D. Huizinga, Non-invasive multimodal functional imaging of the intestine with frozen micellar naphthalocyanines, Nat. Nanotechnol. 9 (8) (2014) 631–638.
[38] J. Yao, J. Xia, K.I. Maslov, M. Nasiriavanaki, V. Tsytsarev, A.V. Demchenko, L.V. Wang, Noninvasive photoacoustic computed tomography of mouse brain metabolism in vivo, Neuroimage 64 (2013) 257–266.
[39] X.L. Deán-Ben, G. Sela, A. Lauri, M. Kneipp, V. Ntziachristos, G.G. Westmeyer, S. Shoham, D. Razansky, Functional optoacoustic neuro-tomography for scalable whole-brain monitoring of calcium indicators, Light Sci. Appl. 5 (12) (2016).
[40] G.A. Malandraki, S. Johnson, J. Robbins, Functional MRI of swallowing: from neurophysiology to neuroplasticity, Head Neck 33 (S1) (2011).
[41] N. Fujii, Y. Inamoto, E. Saitoh, M. Baba, S. Okada, S. Yoshioka, T. Nakai, Y. Ida, K. Katada, J.B. Palmer, Evaluation of swallowing using 320-detector-row multislice CT. Part I: single-and multiphase volume scanning for three-dimensional morphological and kinematic analysis, Dysphagia 26 (2) (2011) 99–107.
[42] D.T. Geddes, L.M. Chadwick, J.C. Kent, C.P. Garbin, P.E. Hartmann, Ultrasound imaging of infant swallowing during breast-feeding, Dysphagia 25 (3) (2010) 183–191.
[43] H.J. Van Staveren, C.J. Moes, J. van Marie, S.A. Prahl, M.J. Van Gemert, Light scattering in Intralipid-10% in the wavelength range of 400–1100 nm, Appl. Optic. 30 (31) (1991) 4507–4514.
[44] K. Homan, S. Kim, Y.-S. Chen, B. Wang, S. Mallidi, S. Emelianov, Prospects of molecular photoacoustic imaging at 1064 nm wavelength, Opt. Lett. 35 (15) (2010) 2663–2665.
[45] Z. ANSI, 136.1 „American National Standard for Safe Use of Lasers, Laser Institute of America, Orlando, 2000.
[46] M. Xu, L.V. Wang, Universal back-projection algorithm for photoacoustic computed tomography, Phys. Rev. 71 (1) (2005), 016706.
[47] J. Gamelin, A. Maurudis, A. Aguirre, F. Huang, P. Guo, L.V. Wang, Q. Zhu, A real-time photoacoustic tomography system for small animals, Opt. Express 17 (13) (2009) 10489–10498.
[48] A. Dima, N.C. Burton, V. Ntziachristos, Multispectral optoacoustic tomography at 64, 128, and 256 channels, J. Biomed. Optic. 19 (3) (2014), 036021.
[49] D. Wang, Y. Wang, W. Wang, D. Luo, U. Chitgupi, J. Geng, Y. Zhou, L. Wang, J.F. Lovell, J. Xia, Deep tissue photoacoustic computed tomography with a fast and compact laser system, Biomed. Optic Express 8 (1) (2017) 112–123.
[50] G. Marquez, L.V. Wang, S.-P. Lin, J.A. Schwartz, S.L. Thomsen, Anisotropy in the absorption and scattering spectra of chicken breast tissue, Appl. Optic. 37 (4) (1998) 798–804.
[51] Y. Zhou, D. Wang, Y. Zhang, U. Chitgupi, J. Geng, Y. Wang, Y. Zhang, T.R. Cook, J. Xia, J.F. Lovell, A phosphorus phthalocyanine formulation with intense absorbance at 1000 nm for deep optical imaging, Theranostics 6 (5) (2016) 688.
[52] X. Dong, W. Yin, J. Yu, R. Dou, T. Bao, X. Zhang, L. Yan, Y. Yong, C. Su, Q. Wang, Z. Gu, Y. Zhao, Mesoporous bamboo charcoal nanoparticles as a new near-infrared responsive drug Carrier for imaging-guided chemotherapy/photothermal synergistic therapy of tumor, Adv. Healthcare Mater. 5 (13) (2016) 1627–1637.
[53] G. Mitic, J. Kölzer, J. Otto, E. Plies, G. Sölkner, W. Zinth, Time-gated transillumination of biological tissues and tissuelike phantoms, Appl. Optic. 33 (28) (1994) 6699–6710.
[54] M. Saxena, S. Sarkar, Involuntary graphene intake with food and medicine, RSC Adv. 4 (57) (2014) 30162–30167.
[55] C.L. Cesar, H. Vargas, C.A.S. Lima, J. Mendes Filho, L.C.M. Miranda, On the use of photoacoustic spectroscopy for investigating adulterated or altered powdered coffee samples, J. Agric. Food Chem. 32 (6) (1984) 1355–1358.
[56] R.C.E. Dias, P. Valderrama, P.H. Março, M.B. dos Santos Scholz, M. Edelmann,

C. Yeretzian, Quantitative assessment of specific defects in roasted ground coffee via infrared-photoacoustic spectroscopy, Food Chem. 255 (2018) 132–138.
[57] A.C. Ailiani, T. Neuberger, J.G. Brasseur, G. Banco, Y. Wang, N.B. Smith, A.G. Webb, Quantitative analysis of peristaltic and segmental motion in vivo in the rat small intestine using dynamic MRI, Magn. Reson. Med. 62 (1) (2009) 116–126.
[58] P.G. Mihai, M. Otto, M. Domin, T. Platz, S. Hamdy, M. Lotze, Brain imaging correlates of recovered swallowing after dysphagic stroke: a fMRI and DWI study, Neuroimage: Clin. 12 (2016) 1013–1021.
[59] T.R. Han, N.-J. Paik, J.W. Park, Quantifying swallowing function after stroke: a functional dysphagia scale based on videofluoroscopic studies, Arch. Phys. Med. Rehabil. 82 (5) (2001) 677–682.
[60] S.G. Rocha, R.G.d. Silva, L.C. Berti, Qualitative and quantitative ultrasound analysis of oropharyngeal swallowing, CoDAS: SciELO Brasil (2015) 437–445.
[61] F.E. Ardakani, Evaluation of swallowing patterns of the tongue using real-time B-mode sonography, J. Contemp. Dent. Pract. 7 (3) (2006) 67–74.
[62] W.J. Dodds, E.T. Stewart, J.A. Logemann, Physiology and radiology of the normal oral and pharyngeal phases of swallowing, AJR Am. J. Roentgenol. 154 (5) (1990) 953–963.